



Jerks abound: An analysis of geomagnetic observatory data from 1957 to 2008



W.J. Brown*, J.E. Mound, P.W. Livermore

School of Earth and Environment, University of Leeds, Leeds LS2 9JT, UK

ARTICLE INFO

Article history:

Received 31 October 2012

Received in revised form 14 May 2013

Accepted 4 June 2013

Available online 19 June 2013

Edited by M. Jellinek

Keywords:

Geomagnetism

Geomagnetic jerks

Secular variation

External field

ABSTRACT

We present a two-step method for the removal of external field signals and the identification of geomagnetic jerks in magnetic observatory monthly mean data, providing quantitative uncertainty estimates on jerk occurrence times and amplitudes with minimal *a priori* information. We apply the method to the complete time series of X-, Y- and Z-components at up to 103 observatory locations in the period of 1957–2008. We find features fitting the definition of jerks in individual components to be frequent and not globally contemporaneous. Identified regional jerks have no consistent occurrence pattern and the most widespread in any given year is identified at <30% of observatories worldwide. Whilst we identify jerks throughout the period of study, relative peaks in the global number of jerk occurrences are found in 1968–71, 1973–74, 1977–79, 1983–85, 1989–93, 1995–98 and 2002–03 with the suggestion of further poorly sampled events in the early 1960s and late 2000s. The mean uncertainties on individual jerk occurrence times and amplitudes are found to be ± 0.3 yrs and ± 2.1 nT/yr², respectively, for all field components. Jerk amplitudes suggest possible periodic trends across Europe and North America, which may be related to the 6-yr periods detected independently in the secular variation and length-of-day.

© 2013 The Authors. Published by Elsevier B.V. Open access under [CC BY license](http://creativecommons.org/licenses/by/3.0/).

1. Introduction

Geomagnetic jerks are conspicuous yet poorly understood phenomena of Earth's magnetic field, motivating investigations of their morphology and the theory behind their origins. Jerks are most commonly defined by their observed form at a single observatory as 'V' shapes in a single component of the geomagnetic secular variation (SV), the first time derivative of the main magnetic field (MF). The times of the gradient changes, which separate linear trends of several years, have associated step changes in the second time derivative of the MF (secular acceleration (SA)) and impulses in the third time derivative. The 'V' shape SV definition of jerks includes an implicit expectation of a 'large' magnitude step change in the gradient without definition of this scale or its threshold value other than the basic need for it to be observable in the data above the highly variable background noise. Jerks can be described by their amplitude, that is, the difference in the gradients of the two linear SV segments about a jerk, $A = a_2 - a_1$, where a_2 is the gradient after the jerk and a_1 is the gradient before the jerk. This mea-

sure is essentially the best fit SA change across a jerk. Jerk amplitude is thus positive for a positive step in SA and negative for a negative step. Here we do not consider spatial extent in our definition and refer to individual features in one field component of a given observatory time series as a single jerk.

The phenomenon of a geomagnetic jerk was first reported by [Courillot et al. \(1978\)](#) as an abrupt turning point separating the otherwise linear trends of the Y(East)-component of SV prior to and after 1970 at several Northern hemisphere observatories (here field components X (North), Y (East) and Z (Vertically-downward) will be referred to throughout). The authors also suggested that events occurred in 1840 and 1910, all corresponding to minima in Earth's rotation rate. The origins of these phenomena were debated primarily by [Malin and Hodder \(1982\)](#), [Malin and Hodder \(1982\)](#) who suggested internal origins, and [Aldredge, 1984](#) who suggested some external component was present in the observatory records. Further spherical harmonic analysis by [Le Huy et al. \(1998\)](#) and wavelet analysis by [Alexandrescu et al. \(1995\)](#) corroborated the now generally accepted view of the internal origin of jerks as a feature of large scale SV. The specifics of internal origins are still debated although jerks are likely linked to the accelerations of core surface flows that generate SV (e.g. [Silva and Hulot, 2012](#)). Recently [Qamili et al. \(2013\)](#) suggested jerks are expressions of more chaotic and unpredictable field behaviour, this may allude to jerks being at the more rapid end of a poorly understood spectrum of core dynamics.

* Corresponding author at: School of Earth and Environment, University of Leeds, Leeds LS2 9JT, UK.

E-mail address: ee07wjb@leeds.ac.uk (W.J. Brown).

Table 1

Overview of key geomagnetic jerk detection works detailing data used, detection technique and events identified (adapted from Pinheiro et al., 2011).

Work	Data	Method	Jerks	Form
Le Mouél et al. (1982)	Annual means (X, Y, Z) 130 observatories	Least-squares (LS) fit two straight lines	1969	Global; amplitudes roughly zonal in X and Z, meridional in Y
Alexandrescu et al. (1996)	Monthly means, combination of X and Y 74 observatories	Wavelet analysis	1901, 1913, 1925, 1932, 1949, 1969, 1978	'69, '78 global with N–S 2-yr delay; '01, '13, '25 possibly global; '32, '45 local
Alexandrescu et al. (1997), Korte et al. (2009)	Various smoothed annual means declination, inclination 1–2 locations	Wavelet analysis, SA zero crossings	Various events 1410–1932	N/A insufficient coverage
Le Huy et al. (1998)	Smoothed annual means (X, Y, Z) 160 observatories	LS fit two straight lines	1969, 1978, 1992	All global; alternating sign; similar distribution of amplitudes
De Michelis et al. (1998), De Michelis et al. (2000)	Annual means (Y), 74 observatories; (X, Y, Z) 109 observatories	LS fit two straight lines	1991	Global; Y amplitude distribution similar to '69, '78
Mandea et al. (2000)	Nine European observatories, monthly means (Y) 12 month running average	Visual	1999	Local
Nagao et al. (2003)	Monthly means (Y) ~50 observatories	Statistical model LS fit two straight lines	1969, 1978, 1991	Global; N–S delay few yrs; '69, '78 show longer duration in South Africa
Chambodut and Mandea (2005)	Monthly means (Y), 12 month running average, 39 observatories, synthetic data from CM4 (Y)	Wavelet analysis/LS fit two straight lines	1971, 1980, 1991	Global but not simultaneous about '71, '80, '91; '91 most complicated structure
De Michelis and Tozzi (2005)	Monthly means (Y), 44 observatories	Wavelet analysis Local Intermittency Measure, LS fit two straight lines	1978, 1986, 1991, 1999	'86 local S Africa and S Pacific, '78, '91, '99 global; '78, '91 show N–S delay
Olsen and Mandea (2007)	CHAMP monthly means (virtual observatories at 400 km altitude)	Spherical Harmonic Expansion/LS fit two straight lines	2003	Simultaneous but local around 90°E
Olsen and Mandea (2008)	xCHAOS	Visual	2005	Local, S Africa
Olsen et al. (2009)	CHAOS-2 monthly means (virtual observatories at 400 km altitude)	Visual	2007	Local, W of Africa
Chulliat et al. (2010)	Monthly means (Y, Z) 5 observatories, CHAOS-2	Visual	2007	Local, Africa; jerks form in pairs from global acceleration pulse at CMB
Pinheiro et al. (2011)	Annual and monthly means and synthetic data from CM4	LS fit two straight lines	1969, 1978, 1991, 1999	'99 local, rest global; no consistency in component pattern; no consistency in global pattern; various regional delays
Qamili et al. (2013)	Synthetic annual Gauss coefficients from Gufm1	Non-linear forecasting	Various events 1600–1980	Chaotic, unpredictable field behaviour

Numerous links have been made between geomagnetic jerk occurrences and other observables, particularly changes in the length-of-day (ΔLOD) (e.g. Holme and de Viron, 2005) and the Chandler wobble (e.g. Gibert and Le Mouél, 2008) suggesting there may be significant angular momentum exchange between the core and mantle as a result of the core flows related to jerks.

The various field derivatives in which jerks can be observed (e.g. MF, SV, SA) mean that a wide variety of detection methods can be employed. A detection method must contend with several factors, for example: noise content in the data, which may be of several origins; the temporal, amplitude and spatial scales at which an event becomes significant enough to be a jerk; the proximity of consecutive jerks; and the asynchronous form of a jerk in each field component. An overview of events detected and the various techniques used are presented in Table 1. A broader summary of studies concerning geomagnetic jerks can be found in Mandea et al. (2010).

This study is structured in the following manner: in Section 2 we introduce a two step method to remove external field noise and to identify jerks in the data; in Section 3 the observatory data are described and the applicability of monthly means is discussed; Section 4 presents the results and their subsequent interpretation before our conclusions are drawn in Section 5.

2. Method

Here we describe a method comprising a combination of two primary components: the removal of external field signals from observatory monthly means after Wardinski and Holme (2011),

and the identification of jerk events in the observatory data based on the premise described by Pinheiro et al. (2011). While SV can be calculated in many ways from MF data, throughout this paper SV will be calculated as the annual difference of monthly means. Annual differences of monthly means was chosen as it reduces the great variability seen in monthly first differences allowing longer term trends to be seen without introducing the smoothing effect which results from methods involving longer period averages. Annual differences of monthly means implies the difference between monthly time samples 12 months apart so that the SV at 6 months between the two measurements is

$$SV(t_{k-6}) = MF(t_k) - MF(t_{k-12}), \text{ with sampling rate } \Delta t_k = 1 \text{ month.} \quad (1)$$

Where annual means are referenced, the SV as first differences of annual means is implied and refers to the difference between a given annual time sample and the previous sample so that the SV at 6 months between the two measurements is

$$SV(t_{k-0.5}) = MF(t_k) - MF(t_{k-1}), \text{ with sampling rate } \Delta t_k = 1 \text{ year.} \quad (2)$$

2.1. External signal removal

Externally generated magnetic signals overlap the periods at which rapid internal field variations occur and thus are a significant noise source for studies of the internal field of the Earth.

A major source of external signals are electrical currents present in the ionosphere and magnetosphere of the Earth. Gubbins and Tomlinson (1986) used magnetic indices of external field activity as selection criteria for generating quiet time monthly means to study jerks, external signal removal from annual means via magnetic indices was applied by De Michelis et al. (1998, 2000) and more recently Verbanac et al. (2007) proposed a method of correcting for external signal in observatory annual means using a combination of field models and magnetic indices. Detailed attempts to parameterise the external field sources as part of field models are documented by e.g. Sabaka et al. (2004) and Olsen et al. (2009), allowing modelled corrections to be applied to observatory data. An alternative to the complex source parameterisations of such models is the statistical approach suggested by Wardinski and Holme (2011).

Wardinski and Holme (2011) document a method to remove SV signals which correlate with the first time derivative of a magnetic index (\dot{D}_{ST} -index (see e.g. Mayaud, 1980)) representing primarily the activity of the magnetospheric ring current (see e.g. Daglis et al., 1999). Alternatively, Wardinski and Holme (2011) showed that the residual between observatory data and a magnetic field model can replace the \dot{D}_{ST} -index in their calculations as a proxy for unmodelled external signals. Removal of such signals was shown to reduce the standard deviation of the data and thus improve the resolution of internal features such as jerks. A full description of the method can be found in Wardinski and Holme (2011), a brief summary of which is given here.

The premise of Wardinski and Holme (2011) is that information regarding external field signals is contained in the unmodelled SV residual between observatory data and the internal magnetic field approximated by a model. Coherent signal between the residuals to the SV of the X-, Y-, and Z-components can be described by a 3×3 covariance matrix, assumed to be constant through time at each given observatory location. The eigenvectors of this residual covariance matrix can then be used to rotate the observed and modelled field components into the directions of least, intermediate and most coherent signal; these directions will be referred to as the 'clean', 'intermediate', and 'noisy' field components and correspond to the eigenvectors with the smallest to largest magnitude eigenvalues, respectively. Wardinski and Holme (2011) showed that the noisy-component at the 50 observatories used in their

study is approximately in the North-South plane. This North-South alignment and a strong zero-lag correlation of the unmodelled residuals in the noisy-component with the \dot{D}_{ST} -index, is consistent with external field signals generated by the equatorial ring current. Additionally, a stronger correlation is seen between the noisy-component residuals at different observatories than to the \dot{D}_{ST} -index, signifying that the index does not fully explain all the unmodelled residual in the noisy-component.

It was proposed by Wardinski and Holme (2011) that a zero-lag correlation based weighting function can be used to remove signal which is coherent between the noisy-component residuals at different observatories, to produce SV time series with reduced external signal content:

$$\dot{r}_{\text{corrected}}(t_k) = \dot{r}_{\text{noisy}}(t_k) - \frac{\sum_l \dot{C}(t_l) \dot{r}_{\text{noisy}}(t_l)}{\sum_l \dot{C}(t_l)^2} \dot{C}(t_k), \quad (3)$$

where $\dot{r}_{\text{corrected}}$ is the corrected noisy-component SV residual, \dot{r}_{noisy} is the noisy-component unmodelled SV residual, \dot{C} is the noisy-component unmodelled SV residual from an alternative observatory and subscripts k and l run over the number of time samples. This correction is applied only to the noisy-component residual before reforming the modelled and unmodelled residual component parts and rotating back to the original X-, Y-, and Z-component directions. This procedure therefore removes signal from the noisy-component residual, which when rotated back to geographic coordinates, results in a removal of signal from each component based on the strength of the correlation to the external signal proxy in each component.

An advantage of this statistical approach over source parameterisation is that it helps to account for the unpredictable nature of local induced fields, that result from heterogeneity in subsurface electrical conductivity. Local induced fields will affect the direction of the external field resulting from features such as the ring current, making their parameterisation difficult (Wardinski and Holme, 2011). As in Wardinski and Holme (2011) we correct for external signal using the residual from the observatory at Niemegk (NGK), Germany, since it provides coverage of the entire timespan of interest with a well documented and reliable record (Niemegk itself is corrected using data from Chambon-la-Forêt (CLF) observatory, France). No other observatory was found to produce

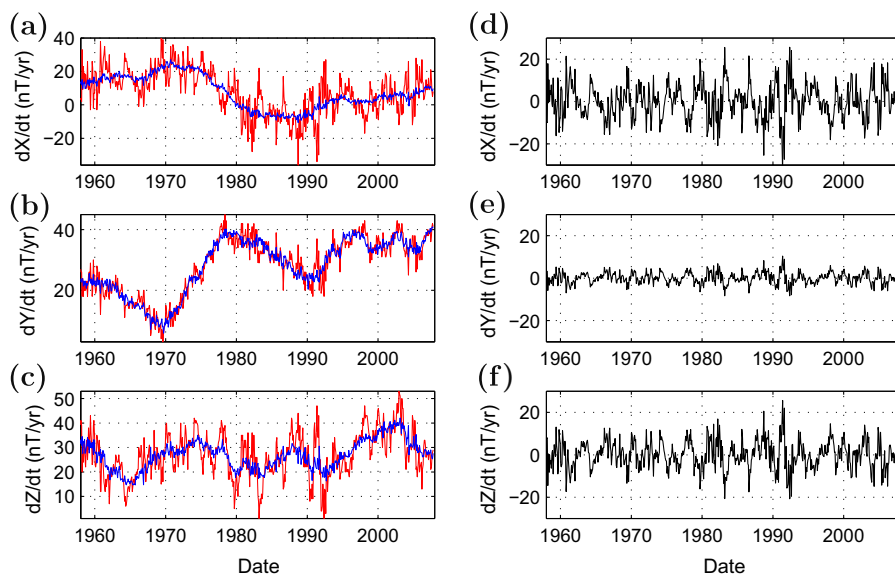


Fig. 1. Original and external field corrected monthly mean SV (a–c) from the observatory at Niemegk (NGK), Germany. Original signal in red and corrected signal in blue. Also shown is the external signal SV removed (d–f) from the original data to produce the corrected signal for the X-, Y- and Z-components (top to bottom).

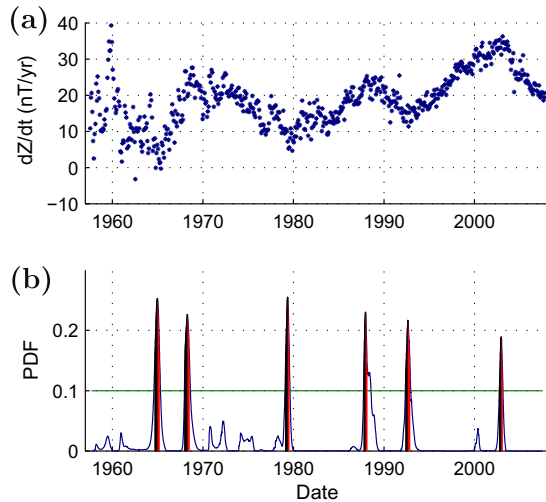


Fig. 2. Example of jerk identification using the sliding window method for the Z-component of SV (a) at Chambon-la-Forêt (CLF), France. PDF function (b) used to identify the most likely jerk times, marked by positive (red) and negative (black) time uncertainties. Jerks are judged to be distinct peaks in the PDF above the cut off value (green line). (For interpretation of the references to colour in this figure legend, the reader is referred to the web version of this article.)

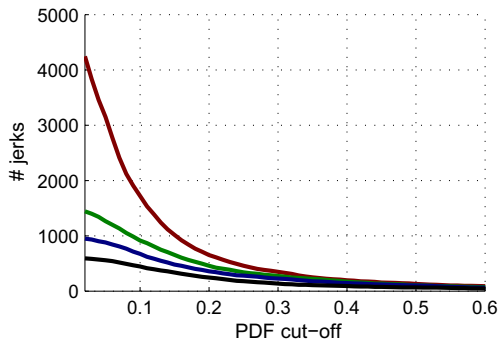


Fig. 3. Trade-off curve of the number of jerks detected versus the probability cut-off threshold above which peaks in probability are to be considered jerks. Curves for jerk detections in all components with a 5-yr (red), 10-yr (green), 15-yr (blue) and 20-yr window (black) are shown. For all window lengths and all individual components a threshold of 0.2 was chosen. (For interpretation of the references to colour in this figure legend, the reader is referred to the web version of this article.)

a significant improvement on the overall results, likely due to the location of Niemegk in central Europe, close to roughly 30% of the observatories used in this study. An example of the improvement made by applying the method to the data is shown in Fig. 1. As expected the greatest signal variation is removed from the X- and Z-components, with limited improvement to the Y-component. The signal removed from each component can be seen to be a scaled version of the same signal, in the case of Fig. 1, the noisy-component SV residual from the relatively nearby CLF observatory. It was found that, averaged over all observatories in our study, signals with mean standard deviations of ± 7 , ± 2 and ± 5 nT/yr were removed from the X-, Y- and Z-components, respectively. The mean peak-to-peak amplitude ranges of these removed signals were 59, 13 and 41 nT/yr for the X-, Y- and Z-components, respectively.

2.2. Jerk identification

Pinheiro et al. (2011) described a method for applying a two-part linear regression to the SV of observatory annual means, generating a probability density function (PDF) of the likelihood of

potential jerk occurrence times. A window of a single component of SV data were selected and the two-part linear regression iterated across the window, considering a potential jerk occurrence at each time step of 0.001 yrs. At each time step, the misfit of the regression to the data was calculated and converted to a probability value to build up the PDF by:

$$\text{PDF}(t_0) \propto \exp \left[-\frac{\chi^2(t_0)(N-3)}{2\chi_{\min}^2} \right], \quad (4)$$

where t_0 is the proposed jerk occurrence time, χ^2 is the least-squares misfit with a minimum value for the window of χ_{\min}^2 , and N is the number of data points in the window.

Assuming Gaussian error distributions about the peaks in likelihood, estimates of the uncertainties in these occurrence times and in jerk amplitudes were calculated. Pinheiro et al. (2011) applied this procedure to selected 11–15 year time windows of data roughly centred about the previously identified jerk occurrences of 1969, 1978, 1991 and 1999 in the X-, Y- and Z-components of 123 observatories worldwide.

Possible events were considered an identified jerk if the PDF function in the time window allowed a 68% confidence window (± 1 standard deviation) to be defined about the most likely occurrence time. Other potential jerks were excluded if a peak in likelihood was seen but the confidence interval could not be contained in the window chosen. If no peak likelihood was seen in occurrence time in the window, no jerk was identified.

2.2.1. Sliding window regression

We propose that the use of a static window of data may bias the identification by severely limiting the extent and time of potential jerk events considered. Methods which utilise complete time series rather than requiring *a priori* data selection (e.g. Stewart and Whaler, 1995; Alexandrescu et al., 1996; De Michelis and Tozzi, 2005) can be seen as more robust in this respect. We thus propose a sliding window, acting as described by Pinheiro et al. (2011), but with the window shifting, one time step per iteration, along the series being considered and the PDF calculation repeated. A summation of the resulting overlapping functions produced can then be normalised (to an integral of 1) to give a continuous PDF for the entire series which has considered each possible jerk time at every relative time in a window (Fig. 2). This removes the bias towards events centred in the window and also removes any potential bias arising from manually selected window times.

The time uncertainty estimation procedure of Pinheiro et al. (2011) (uncertainties are taken to be ± 1 standard deviation of each PDF peak, assumed to be Gaussian) can still be applied to peaks in the PDF but we introduce the addition of a threshold probability above which events are deemed significantly likely compared to the background level of likelihood which results from the misfit to the variability in the data. A threshold of 0.2 was chosen based on a trade-off curve of the number of jerks identified versus the probability threshold (Fig. 3). This threshold assumes that the relatively high peaks in the jerk time PDFs are the most sound estimates of jerk times and was set slightly to the right of the knee of the trade-off curve (Fig. 3) to reduce the likelihood of false positives.

This method moves towards identification of jerk-like trends in SV with minimal *a priori* information required; nevertheless some assumptions are made and limiting parameters imposed to counter the issues of the jerk identification problem. It is assumed that: a jerk takes the form of an instantaneous change in the gradient of SV (a step in SA); that there is a minimum jerk amplitude below which events are not considered likely to be jerks; and that the misfit of the jerk model to the data can be related to the probability

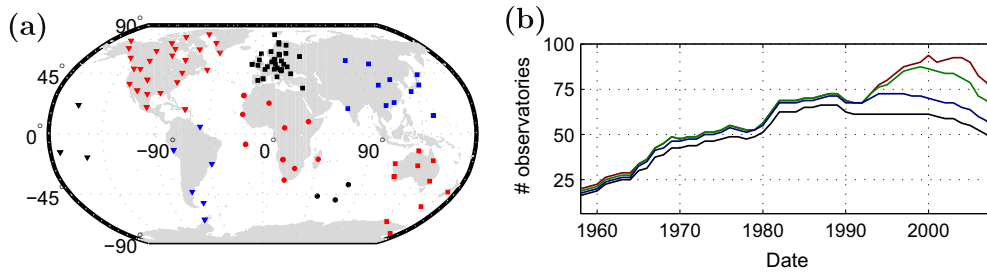


Fig. 4. Map showing observatory locations used in this study (a). The 8 groups of symbols show regions of observatories as described in Section 4. While all the observatories highlighted above were used in this study, not all were operating throughout the entire period of interest, (b) shows the number of observatories operating in any given six month period between 1957 and 2008. The number of observatories providing minimum length time series of 5 yrs (red), 10 yrs (green), 15 yrs (blue) and 20 yrs (black) are shown. (For interpretation of the references to colour in this figure legend, the reader is referred to the web version of this article.)

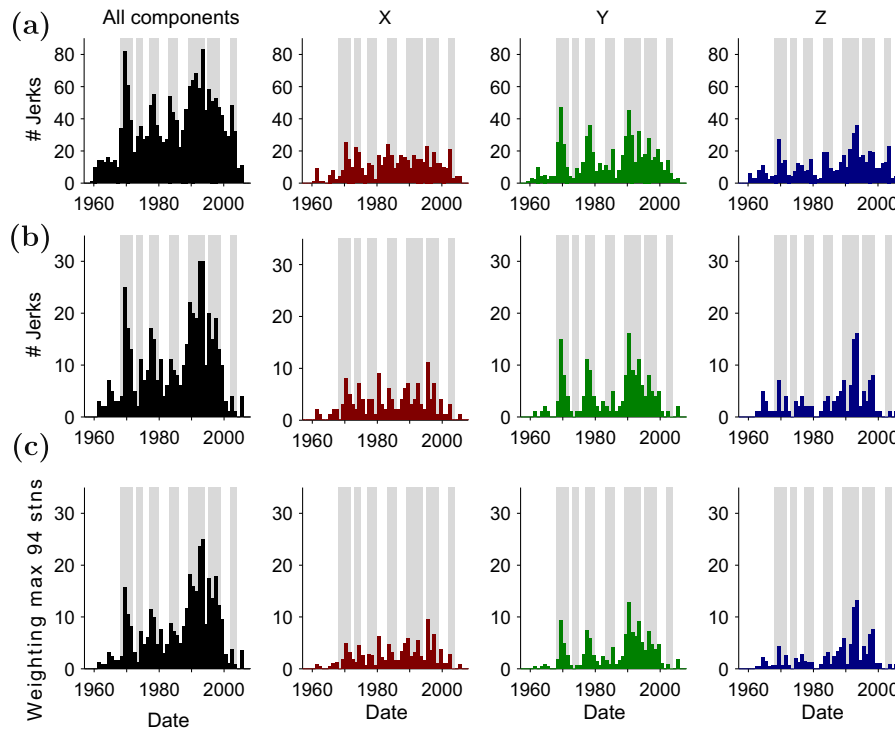


Fig. 5. Histograms of detected jerks in 12-month time bins between 1957 and 2008, (a) shows straight counts when results from 5-, 10-, 15- and 20-yr windows are combined, (b) shows straight counts for a 10-yr window, (c) shows 10-yr window counts weighted by the number of operating observatories during any given time bin. Columns represent from left to right: the collation of all components, X-component only, Y-component only, Z-component only. The maximum possible weighting value is indicated by the maximum number of observatories (stns) on the y-axis label; this maximum represents a jerk detected at every observatory. Detections at all observatories worldwide are included, grey bands indicate times of peaks in combined (black) histogram for all window lengths (a).

of that model representing the data by Eq. (4) both for sections of data in which jerks are present or absent.

In addition to the threshold probability mentioned previously, a magnitude of 3 nT/yr^2 was chosen as the minimum jerk amplitude which is recognised as a significant trend above the variability of the background noise level in the data. Since it is not assumed that a jerk is present in each window, this limit is required to impose zero probability on features such as long linear sections of data, which otherwise show a low misfit when both sections of the linear regression align approximately parallel to each other. Amplitude best estimates are taken to be the value which produces the lowest misfit to the data when considering the range of amplitude estimates from all time windows which identify a given time as a potential jerk. The uncertainties on amplitude estimates are then calculated as the differences between the best estimate and the

maximum and minimum values of the range of amplitude estimates.

The length of the time window in which data is considered during each linear regression must also be imposed. It was decided to utilise a variety of window lengths as a reassurance of the robustness of identified events due to the limiting role the window length plays in the resolution of consecutive events. Consecutive jerks which occur within a single window length are less likely to be resolved individually. Thus jerks were identified with window lengths of 5, 10, 15 and 20 yrs. The time step occurrences at which possible events are considered must be defined, this was chosen to be 0.001 yr as used by Pinheiro et al. (2011) since this sampling rate is sufficiently higher than the monthly (0.08 yr) data sampling and produces smooth PDFs. All input parameter values were chosen after testing using both synthetic and real data.

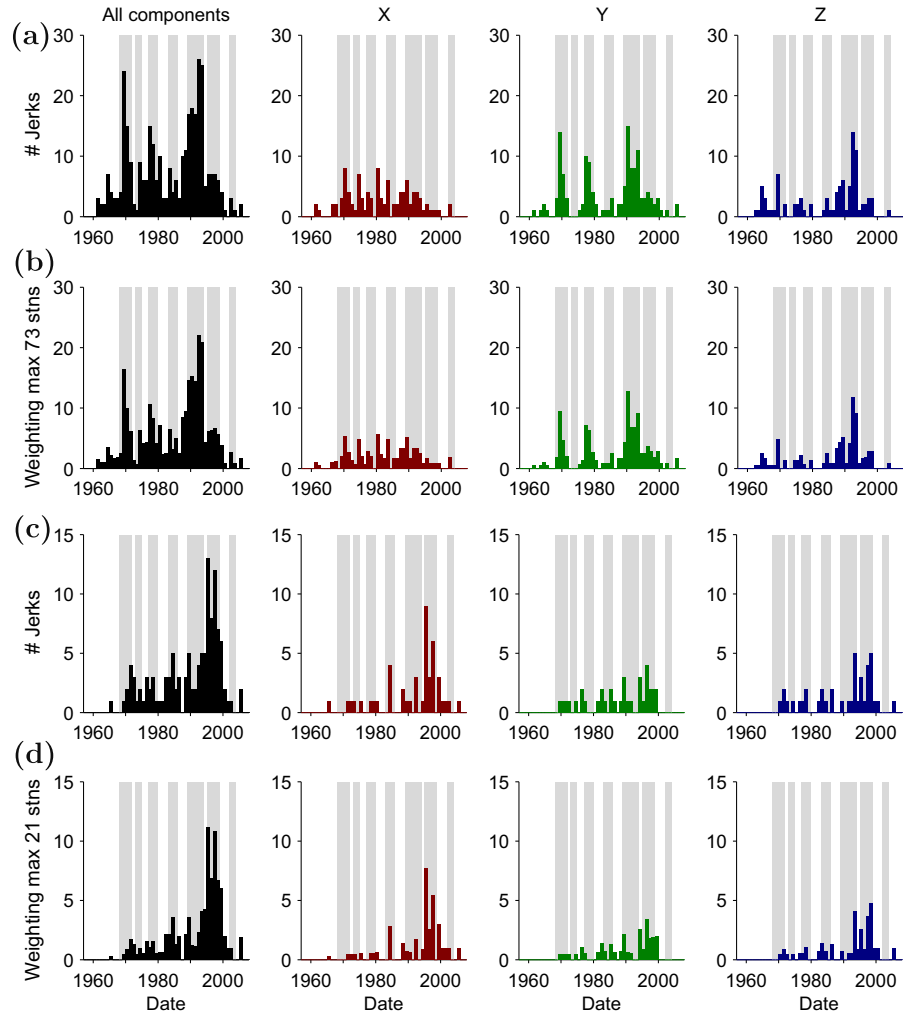


Fig. 6. As Fig. 5 but for observatories in the Northern hemisphere ((a) count, (b) weighted) and Southern hemisphere ((c) count, (d) weighted) only.

This method thus provides a means of consistently identifying features which statistically fit the definition of a jerk in the SV. It is also able to provide a relative probabilistic weighting with which to consider the identified events as constrained by the data, and a quantitative estimate of the uncertainties in times and in jerk amplitudes.

3. Data

Monthly mean MF data were obtained from the Bureau Central de Magnétisme Terrestre (BCMT), World Monthly Means Database Project. This database comprises full monthly averages of all hourly mean values for the X-, Y-, and Z-components at 118 observatories worldwide and was compiled by Chulliat and Telali (2007) from hourly means, initially obtained from the World Data Centre (WDC) for Geomagnetism at the British Geological Survey, Edinburgh. Further to the consistency checks of Chulliat and Telali (2007), we have applied all documented baseline corrections and accounted for gaps of unrecorded data in one of two ways. Gaps shorter than 6 months were interpolated using a linear fit to the field component in question. A minimum of 12 months of data either side of a gap was required for interpolation to be performed. For gaps longer than 6 months the records were split into separate time series on either side of the gap and will be considered as individual records from here on.

When considering analysis of observatory data it is important to consider the dependence of any interpretation on the spatial and temporal distribution of the data upon which it is founded. It is well known that observatory data provide spatial sampling biased heavily towards continental regions, particularly Europe and North America, and that the density of observations varies through time, generally increasing towards the present day as more observatories have been established (see Fig. 4).

The procedure described in detail in Section 2.1 requires use of a magnetic field model. For this purpose C³FM2 of Wardinski and Lesur (2012) was used. The model is a fit to observatory SV over the period of 1957.0–2008.4, further constrained by satellite field models in 1980 and 2004. As such it provides coverage specifically tailored to SV across the period in which observatory data is most widely available. The data timespan of this study was thus constrained by the model length. While observatory data are available extending back to the late 1800s, the spatial coverage is too limited for our study. While C³FM2 was chosen for this study, the methods described in Section 2 are, in principle, applicable to any period for which observations and models are available.

3.1. Data sampling

We suggest that when investigating rapid, sharp features such as jerks it is preferable to utilise monthly sampling of observatory

data with as little smoothing as possible to achieve the best time resolution. Annual mean observatory data were used by [Pinheiro et al. \(2011\)](#) in preference to monthly means due to the greater availability of stations and the view that monthly means, in the form of 12 month running means of first differences in dipole coordinates (X- and Y-components rotated to be parallel and perpendicular to the dipole axis), contain correlated external noise as well as much greater variability. The correlated external signal in this case breaks the assumption of Gaussian error distributions and the high variability leads to unacceptable misfit of linear trends to the data. It was also noted by [Pinheiro et al. \(2011\)](#) that jerks appeared to be more contemporaneous between field components when considering annual means.

We find that spatial coverage of observatory data, while generally poor, is not greatly reduced by considering monthly means over annual means. In this study 96 observatories were used when considering an 11- to 15-yr window length as used by [Pinheiro et al. \(2011\)](#) who utilised 123. Of the 27 additional stations used by [Pinheiro et al. \(2011\)](#), the majority are short Northern hemisphere records in the late 20th to early 21st century and do not greatly influence the spatial or temporal distributions of data used. For window lengths of 5 yrs, 103 observatory locations were found to be suitable whilst for windows of 20 yrs, 76 observatory records were available.

The assumption that monthly means contain too much correlated signal which is not present in annual means ([Pinheiro et al., 2011](#)) is best addressed via an example. Considering the observatory record from Niemegk (NGK), Germany, during the period of the C³FM model, the 3×3 covariance matrix (D_{annual}) of annual means unmodelled SV residuals (X-, Y-, Z-components) and its corresponding normalised eigenvectors (v) and eigenvalues (λ) are found to be (to one decimal place)

$$D_{\text{annual}} = \begin{bmatrix} 17.2 & -5.5 & -14.7 \\ -5.5 & 2.1 & 4.0 \\ -14.7 & 4.0 & 28.7 \end{bmatrix} (\text{nT/yr})^2,$$

$$v_{\text{clean}} = \begin{bmatrix} 0.4 \\ 0.9 \\ 0.0 \end{bmatrix}, \lambda_{\text{clean}} = 0.3 (\text{nT/yr})^2,$$

$$v_{\text{intermediate}} = \begin{bmatrix} -0.8 \\ 0.3 \\ -0.6 \end{bmatrix}, \lambda_{\text{intermediate}} = 7.9 (\text{nT/yr})^2,$$

$$v_{\text{noisy}} = \begin{bmatrix} -0.6 \\ 0.2 \\ 0.8 \end{bmatrix}, \lambda_{\text{noisy}} = 39.8 (\text{nT/yr})^2,$$
(5)

while for monthly means unmodelled SV residuals the covariance matrix (D_{monthly}), eigenvectors and eigenvalues are found to be

$$D_{\text{monthly}} = \begin{bmatrix} 79.8 & -25.5 & -58.0 \\ -25.5 & 10.0 & 18.0 \\ -58.0 & 18.0 & 66.4 \end{bmatrix} (\text{nT/yr})^2,$$

$$v_{\text{clean}} = \begin{bmatrix} 0.3 \\ 0.9 \\ 0.0 \end{bmatrix}, \lambda_{\text{clean}} = 1.6 (\text{nT/yr})^2,$$

$$v_{\text{intermediate}} = \begin{bmatrix} -0.6 \\ 0.2 \\ -0.8 \end{bmatrix}, \lambda_{\text{intermediate}} = 15.6 (\text{nT/yr})^2,$$

$$v_{\text{noisy}} = \begin{bmatrix} -0.7 \\ 0.2 \\ 0.6 \end{bmatrix}, \lambda_{\text{noisy}} = 139.0 (\text{nT/yr})^2.$$
(6)

The covariance matrices describe the coherency of signal between the X-, Y-, and Z-components and have associated eigenvectors and eigenvalues which describe, respectively, the directions and magnitudes of these signals. Comparing Eqs. (5) and (6) it can be seen that the eigenvalues are of greater magnitude and thus the coherency of signal is greater for monthly means while the eigenvectors are in similar directions for both annual and monthly data. This shows that while reduced in magnitude, the coherent signal is not removed by calculating annual means. As expected, the reduced covariance seen with annual means is only from the reduction in variability of the signal overall. These two cases can be compared to the covariance matrix ($D_{\text{corrected monthly}}$), eigenvectors and eigenvalues of monthly means unmodelled residuals once external signal is accounted for as described in Section 2

$$D_{\text{corrected monthly}} = \begin{bmatrix} 2.0 & -0.2 & 2.6 \\ -0.2 & 2.6 & -1.4 \\ 2.6 & -1.4 & 3.7 \end{bmatrix} (\text{nT/yr})^2,$$

$$v_{\text{clean}} = \begin{bmatrix} -0.7 \\ 0.3 \\ 0.6 \end{bmatrix}, \lambda_{\text{clean}} = -0.1 (\text{nT/yr})^2,$$

$$v_{\text{intermediate}} = \begin{bmatrix} 0.4 \\ 0.9 \\ 0.1 \end{bmatrix}, \lambda_{\text{intermediate}} = 2.3 (\text{nT/yr})^2,$$

$$v_{\text{noisy}} = \begin{bmatrix} 0.5 \\ -0.3 \\ 0.8 \end{bmatrix}, \lambda_{\text{noisy}} = 6.0 (\text{nT/yr})^2.$$
(7)

It is clear that there is much improvement with the removal of coherent unmodelled signal: smaller eigenvalues imply less coherent signal than for untreated annual or monthly data. The eigenvectors, the direction of the dominant coherent signal, are also altered and no longer show the same contaminating ring current effects with the cleanest component direction now close to that of the original noisy component. With little covariance between the field components, the assumption of Gaussian errors made by [Pinheiro et al. \(2011\)](#) can hold for monthly data, making them suitable for this study. The denser sampling leads to greater accuracy in time identification of jerks since the process of calculating annual means from monthly means introduces a smoothing to the data, rounding off the sharp features of jerks to create a broader apex in the SV.

4. Results

Due to the large amount of data involved and the wide extent of results generated, only the key results are summarised here. The full results of the identified jerks from this study are available in the [Supplementary material](#). This resource includes data files containing all identified jerk times with associated properties such as uncertainties, probabilities and jerk amplitudes as well as additional figures and movies of jerk identifications through time.

For all window lengths the numbers of jerks were found to be roughly equal in each field component. While the mean event probability increased with the window length due to lower numbers of jerks being detected, the median probability was found to be independent of window length and equal in all components at a value of ~ 0.3 . Overall the number of individual events identified varied depending on the window length used with a maximum of 651 detected with the 5-yr window and 244 detected with the 20-yr window. For brevity, only results from the 10-yr window are depicted in subsequent figures as they are deemed representative of the major features in the data. The uncertainty estimates on the identified jerk times were also found to increase with window length from ± 0.2 yrs with a 5-yr window to ± 0.4 yrs with a

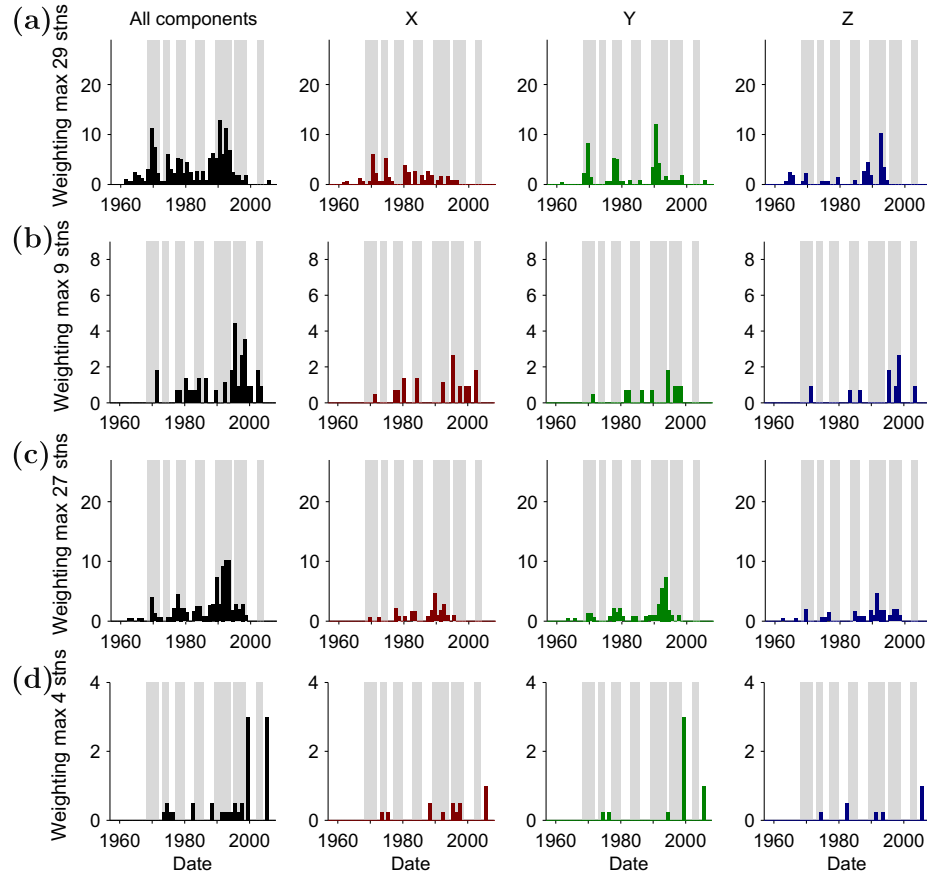


Fig. 7. Weighted histograms as Fig. 5 but for observatories in (a) Europe, (b) Africa, (c) North America and (d) South America only.

20-yr window in all components. These values nevertheless show that the use of monthly mean data has indeed increased the time resolution of jerk events compared to previous studies (mean uncertainties of ± 1.4 yrs were found by Pinheiro et al. (2011)). The positive and negative uncertainties were found to be symmetrical and therefore consistent with the assumption of Gaussian error distributions. The uncertainty estimates were also found to be approximately constant through the time period studied. The mean uncertainty estimates of jerk amplitudes were found to be on the order of ± 2.1 nT/yr². As noted by Pinheiro et al. (2011) jerk amplitudes are a robust measure with the sign of contemporary jerk amplitudes at nearby observatories seen to be consistent.

4.1. Temporal distribution

The timing of jerks is here assessed by histograms of occurrences through time for a variety of spatial regions to assess the robustness of the idea of specific global or local events. A series of straight histogram counts and of equivalent weighted histograms were calculated. The weighted count (Eq. (8)) is calculated as the number of identified jerks in a time bin ($n_{\text{detections}}$) multiplied by the ratio of the number of active observatories in a given time bin ($\text{obs}_{\text{active}}$) to the maximum number of observatory locations in the study ($\text{obs}_{\text{total}}$):

$$W_{\text{bin}} = n_{\text{detections}} \frac{\text{obs}_{\text{active}}}{\text{obs}_{\text{total}}} \quad (8)$$

Whilst it may seem contradictory to down-weight the significance of high proportions of detections at low numbers of active observatories, the weighting is designed to favour observations at the greatest number of observatories to assess whether identifying global events is a justified conclusion. The uncertainty in the time

occurrence of each identified event is assumed to be inconsequential for the histograms provided the time bins are wider than the magnitude of the uncertainty estimates, thus a minimum bin width of 12 months is used.

Since the different window lengths used in the identification procedure favourably resolve features at different timescales, a combined histogram of results from all window lengths is shown (Fig. 5a). This was used to identify the periods of most frequent jerk activity. Relative peaks can be seen in 1968–71, 1973–74, 1977–79, 1983–85, 1989–93, 1995–98 and 2002–03 with additional suggestions of events in the early 1960s and the late 2000s. These periods fall at the ends of the data set and thus suffer a lack of resolution from edge effects of the identification procedure. Additionally, the early 1960s are poorly resolved spatially due to this period having the lowest coverage of observatories in this study. The histograms in Figs. 5–8 show that in general the proportion of observatories at which events are identified at a given time is low. Considering all components at all observatories included in the study worldwide, the most widespread jerk identified is seen in 1989–93 at $\sim 30\%$ of the observatories (Fig. 5b). The predominant peaks in the global histogram (Fig. 5a, combined component histogram) represent both a combination of events from all field components e.g. in the 1990s, and also exceptionally high counts from a single component e.g. 1977–79 in the Y-component. These peaks can also be the result of contributions from various regions at overlapping times to produce a peak in the global histogram. When only observatories which are located in the Northern or Southern Hemisphere are considered (Fig. 6) it can be seen that events in the Northern Hemisphere dominate the global distribution due to the contribution from 73 observatories compared to 21. While the Northern Hemisphere (and thus global) results can in places be described as showing individual peaks of high numbers of jerks

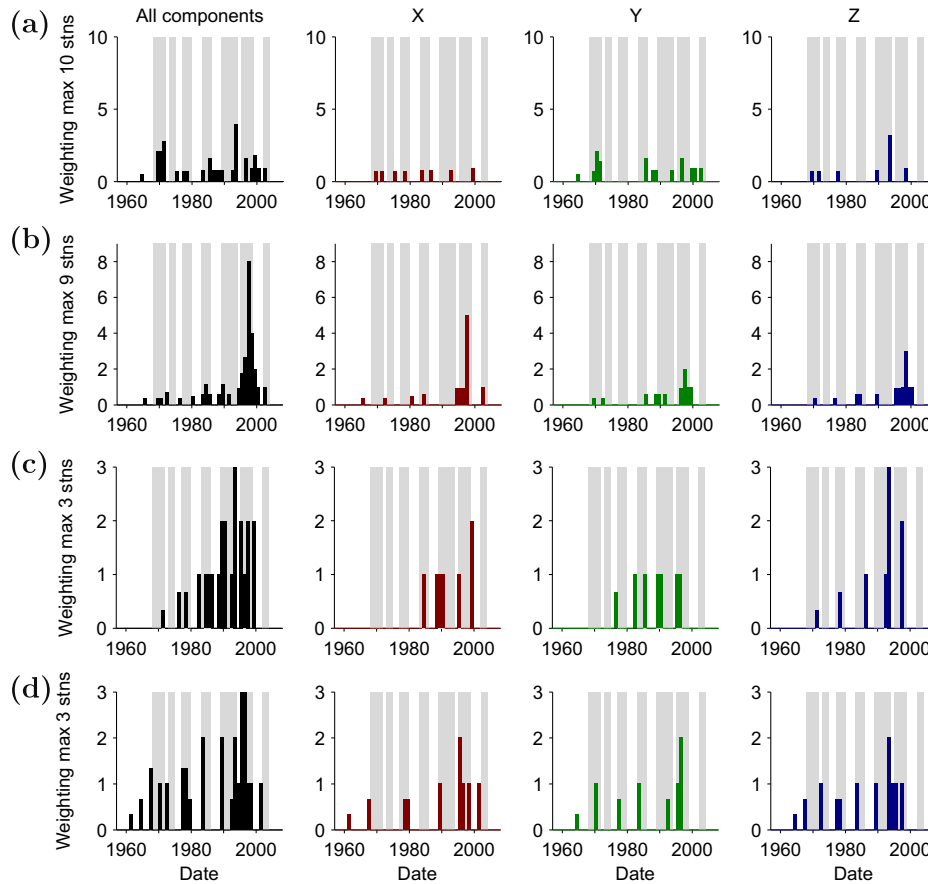


Fig. 8. Weighted histograms as Fig. 5 but for observatories in (a) Asia, (b) Australasia, (c) Southern Indian Ocean and (d) Pacific Ocean only.

detected in a short period of time, the Southern Hemisphere results do not mirror this pattern. This is potentially due to the lack of data rather than the absence of events. A point of interest is that a peak is seen around 1968–1971 in both hemispheres which does appear to fit the reported observation of an event occurring in the Northern Hemisphere 1–3 yrs before the Southern Hemisphere (Alexandrescu et al., 1996). This trend of short North-South delay is not seen for any other distinct peaks and does not appear to be a consistent feature of jerks although the events in 1989–93 and 1995–98 are observed to be largely hemispheric. It is likely that these periods represent two or more regional events overlapping in time, a common feature of the peaks in the global histograms.

The global time distribution of jerks can be broken down further into jerks occurring in spatially distinct regions of observatories (shown on Fig. 4a). The regional histograms for observatories in Europe, Africa, North America and South America (Fig. 7) and Asia, Australasia, the Southern Indian Ocean and the Pacific Ocean (Fig. 8) show which particular components in which regions contribute to the globally observed trends. For example, the distinct global peak around 1969 is predominantly a feature of the X- and Y-components in Europe, the only other significant contributions coming from the Y-components in North America and Asia. We find the event to be very poorly constrained in the Southern Hemisphere.

The global peak around 2003 (Fig. 5a) appears only weakly in the results for the 10-yr window (Figs. 5(b) 6,7,8), due to the short timescale of the features in the SV post 2000 and the proximity to the end of the data set. As such, detections are limited with windows of 10-yr and longer but frequent with the 5-yr window. Proximity to the end of the data set is likely also the reason we do not resolve the 2005 (Olsen and Mandea, 2008) and 2007 (Olsen

et al., 2009; Chulliat et al., 2010) events. Visual inspection of time-series suggests that events on a similar scale to those post 2000 may also occur in the early 1960s, producing small peaks in the histograms (Fig. 5). These time periods may benefit from a more focused study.

The 1990s show a high incidence of identified events across all regions, focused in the Y- and Z-components in the Northern Hemisphere in 1989–93 and the X- and Z-components in the Southern Hemisphere in 1995–98. These periods may host several events, the overlapping durations of which prevent the definition of a sharp peak. The focus of the latter of these two peaks in the poorly sampled Southern Hemisphere may explain the previous uncertainty over the extent of the mooted 1999 jerk (De Michelis and Tozzi, 2005; Pinheiro et al., 2011).

Further distinct events are difficult to trace between regions, being detected in various components in various regions with the dominant signal coming from European observatories.

4.2. Spatial distribution and morphology

Despite the fact that generally only a small proportion of observatories identify jerks in a given time period, it is still informative to look at the spatial distributions of these events. As noted by Pinheiro et al. (2011), the jerk amplitudes prove to be a reliable measure, showing that even where low probability events are identified, the uncertainty estimates are small and the amplitudes of events detected at observatories in close proximity show the same polarity and similar magnitude.

Examples of the amplitude distributions for three characteristically different regions of peaks in the histograms seen in Section 4.1 are depicted here: a well documented global peak whose precise

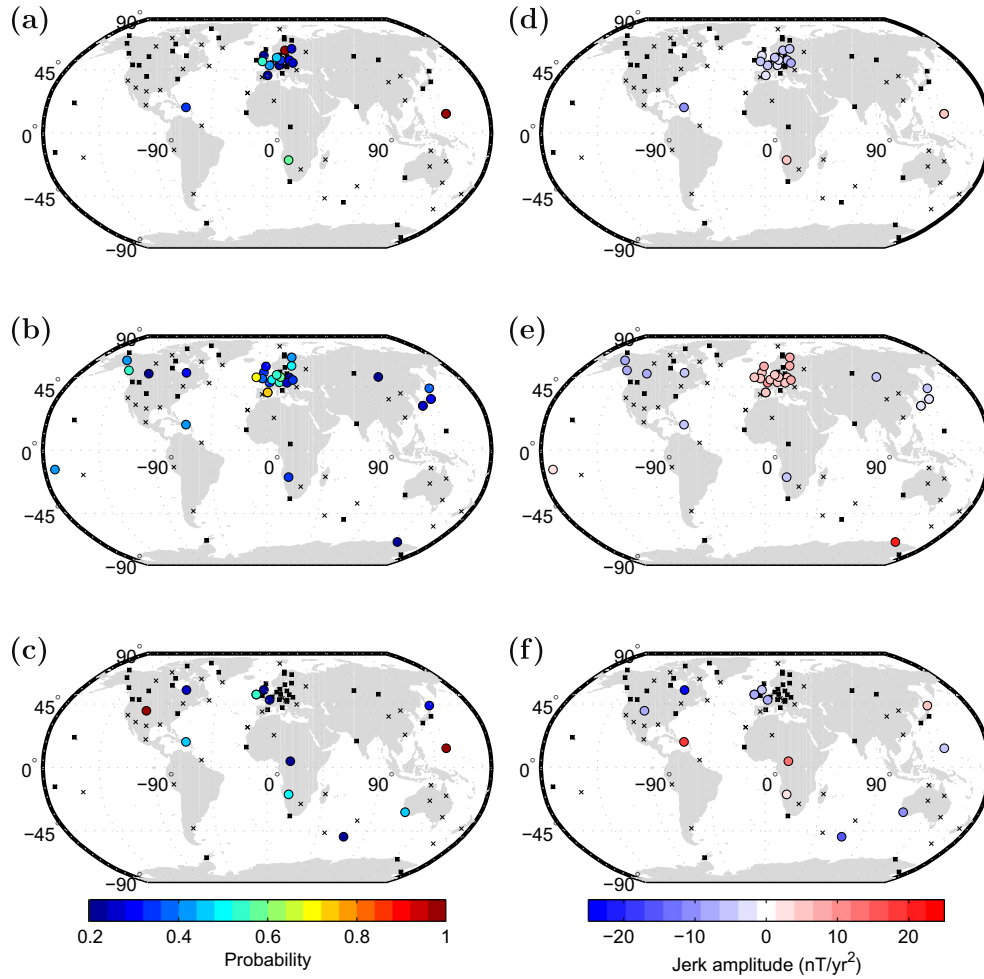


Fig. 9. Jerk probability (a–c) and amplitudes (d–f) for the period of 1968–1971. Top to bottom are the X-, Y- and Z-components, respectively. Black crosses represent inactive observatory locations, black squares represent active observatory locations which did not detect a jerk and coloured circles represent identified jerks. Results from 10-yr window.

occurrence time varies by region (1968–71, Fig. 9); a broad period of the highest incidence of events in all components in all regions (1989–93, Fig. 10); and a period which contains an event whose extent is debated between various studies (1995–98, Fig. 11). For equivalent figures of the remaining periods of relative peaks in jerk occurrences, we refer the reader to the [Supplementary material](#).

The jerk amplitudes of 1968–71 (Fig. 9) are seen to be dominated by Northern Hemisphere, particularly European, observations in the X- and Y-components. The X- and Y-components show similar spatial and magnitude patterns but with opposite polarity. There is no evidence of the zonal patterns in X- and Z-components or the sectoral pattern in the Y-component as described by early works such as [Le Mouél et al. \(1982\)](#). The Z-component is largely unconstrained over Europe and a much less significant event than those in the X- and Y-components. Our amplitude results fit well with those calculated for the 1969 jerk by [Le Huy et al. \(1998\)](#), [De Michelis et al. \(2000\)](#) and [Pinheiro et al. \(2011\)](#) and disagree with those of [Le Mouél et al. \(1982\)](#) in so doing. Little can be determined conclusively about the morphology in the Southern Hemisphere.

The jerk amplitudes in the period of 1989–93 (Fig. 10) show a different style from those of 1968–71. Jerks are seen more consistently across wider regions in all three components. There is a very high incidence of jerks in all three components at overlapping

times during the 5-yr period of 1989–93. Twin peaks of 1–3 yrs in jerk occurrences are seen in the X-, Y- and Z-components in an asynchronous manner, leading to an overall peak spanning 1989–93 (Figs. 5–8). The resulting pattern of amplitudes is more complicated than that of 1968–71, with localised variations in polarity. The jerks in the Y-component in Europe appear to transition from positive to negative polarity through time while the X- and Z-component occurrences peak twice with the same polarity. Observations in X- and Y-components in North America appear to transition between positive and negative amplitudes spatially with all jerks occurring in a single span of 2–3 yrs. Our results suggest the complicated structure and varying descriptions of the reported 1991 jerk (see [Le Huy et al., 1998](#); [Chambodut and Manda, 2005](#); [De Michelis and Tozzi, 2005](#)) can be explained by a double peak in the occurrences of jerks in our results in the period of 1989–93. Our amplitude results from the latter half of the 1989–93 peak best agree with the 1991 jerk amplitudes of [Le Huy et al. \(1998\)](#), [De Michelis et al. \(2000\)](#) and [Pinheiro et al. \(2011\)](#).

Jerk amplitudes in the period of 1995–98 (Fig. 11) are unusual with respect to other periods of frequent jerk occurrences in that most of our detections are in the Southern Hemisphere. Our amplitude results are consistent with those of [Manda et al. \(2000\)](#), [De Michelis and Tozzi \(2005\)](#) but not those of [Pinheiro et al. \(2011\)](#). We find minimal evidence of jerks in Europe, and more widespread occurrences in the rest of the world whilst [Pinheiro et al., 2011](#)

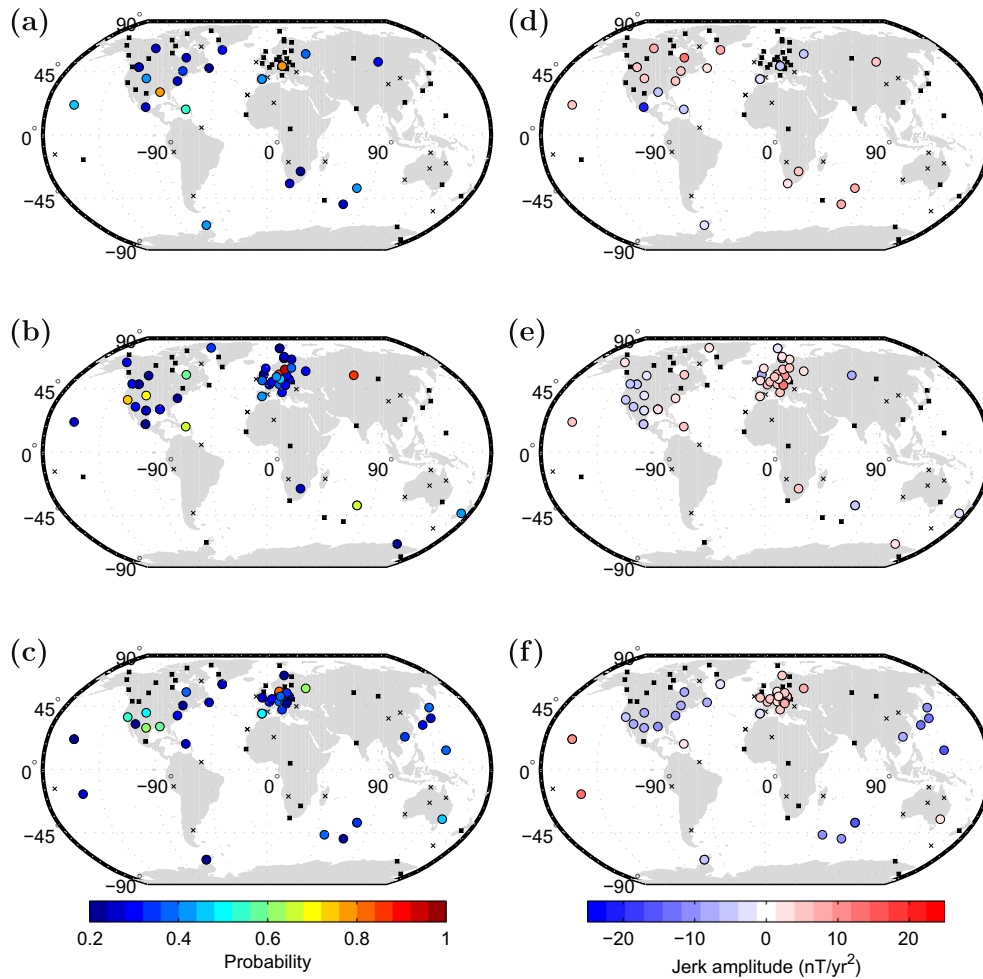


Fig. 10. As Fig. 9 but for the period of 1989–1993.

found very limited local evidence, largely in Europe. This discrepancy may be a result of the limited data window of 11–15 yrs of annual means selected by Pinheiro et al. (2011) which was centred around 1999 and thus possible overlap of events in the early to mid 1990s and 2000s, which we define as temporally close but distinct periods of frequent jerk occurrences.

A peak in the occurrences of jerks is seen in the period of 1977–79 (Figs. 5–8), comparable to the 1978 jerk and corresponding amplitudes observed by De Michelis et al. (1998), Le Huy et al. (1998) and Pinheiro et al. (2011) in all components. The observations of this period bear much similarity to those of 1968–71 including providing few constraints of events in the Southern hemisphere.

The jerks in the period of 2002–03 (Fig. 5a and Supplement) are seen in all three components. As mentioned in Section 4.1, the proximity to the end of the data set means that few events are seen with a window of 10 yrs or longer and jerks are more readily identified with the 5-yr window. A unique characteristic of this time period is that all the observations of the Z-component suggest a strong hemispheric dichotomy in polarity (see Supplement), a feature not seen in any other period investigated. Our amplitude results here agree with the observations of Olsen and Manda (2007) in all three components.

The reported 2005 (Olsen and Manda, 2008) and 2007 (Olsen et al., 2009; Chulliat et al., 2010) jerks are not prominent in our results; this is likely due to the reduced effectiveness of our identification method with proximity to the end of the data set. Observed

amplitude patterns do not appear to be consistent in form between events although regional polarity does seem to show an alternating pattern. This will be discussed in Section 4.4.

4.3. Spatiotemporal relationship

The relationship between the temporal and spatial patterns of jerk occurrences could hold information as to their source mechanism. For example jerks generated by torsional oscillations (e.g. Bloxham et al., 2002) may show evidence of wave propagation in the cylindrically radial direction. The presence of trends in identified jerk times with cylindrical radius (or latitude) and longitude were investigated. No clear relationships were found in any combination of these variables. It was found that accounting for the concentration of observatory locations in certain regions, jerk times appear to be distributed evenly through latitude, longitude or cylindrical radius and concentrated only about certain time periods as Figs. 5–8 show. It can be seen in Fig. 12 that while some epochs, e.g. around 1970 in the Y-component, show a more dense clustering in time of jerks at a range of cylindrical radii, there is no consistent pattern between the events which correspond to relative peaks in the histograms in Figs. 5–8.

4.4. Periodicity of jerk amplitude

It has been observed (e.g. Le Huy et al., 1998; Chulliat et al., 2010) that the series of jerks at approximately 1969, 1978 and

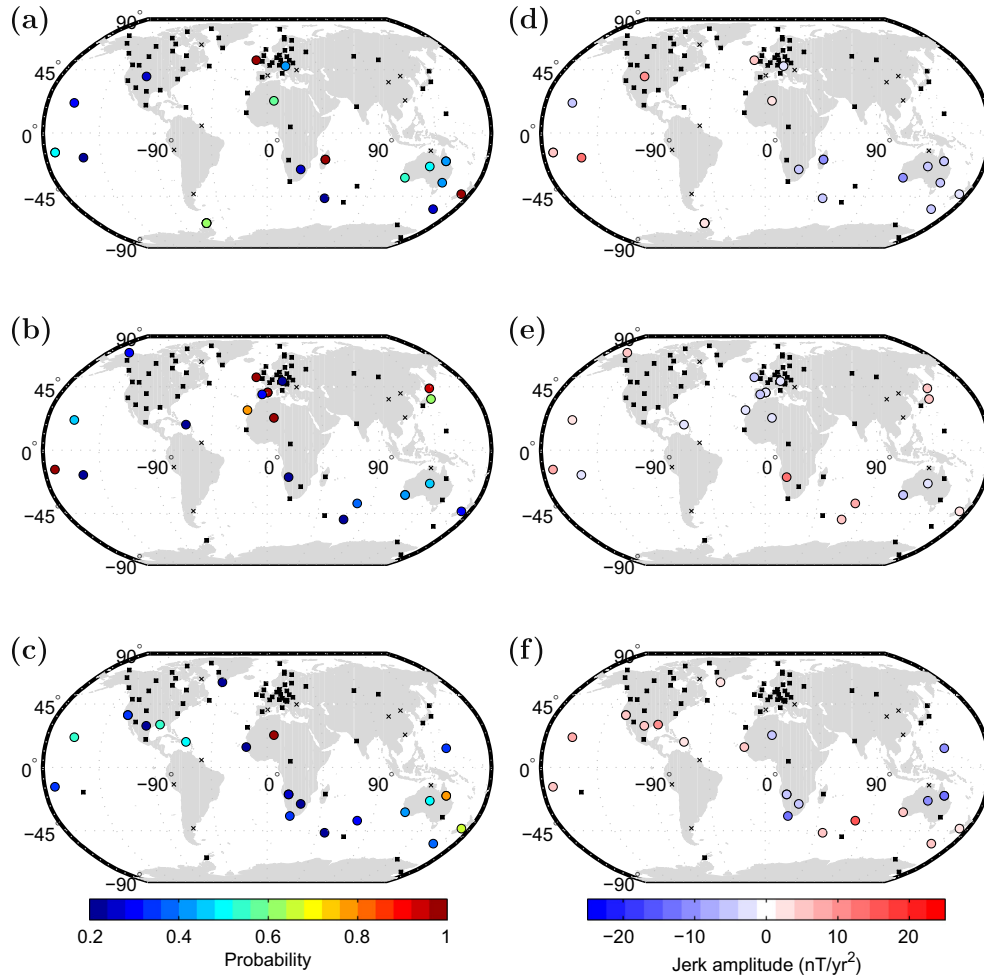


Fig. 11. As Fig. 9 but for the period of 1995–1998.

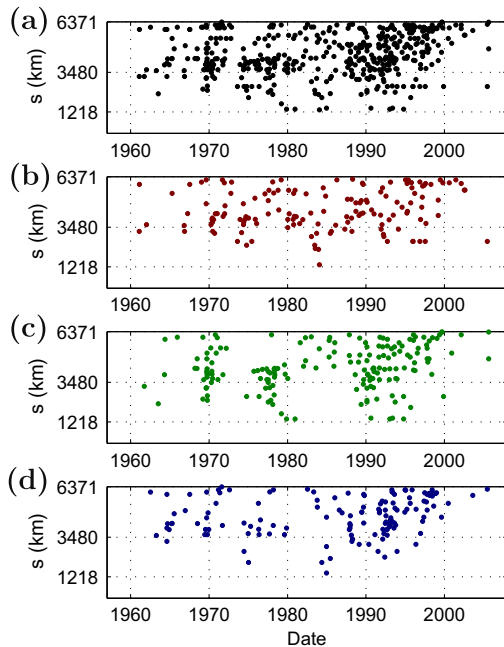


Fig. 12. All identified jerk occurrences using a 10-yr window plotted against cylindrical radius (s). Plots show jerks in (a) all three components and in the individual (b) X-, (c) Y- and (d) Z-components.

1991 show a trend of alternating polarity of jerk amplitude. It has been suggested this is a feature of long term memory in the source mechanism of jerks (e.g. Alexandrescu et al., 1996; Le Huy et al., 1998). With regard to analysing this trend in our results three questions arise: are successive jerks seen to change amplitude polarity through time? Is this trend zero mean? Is this polarity change periodic? The amplitude maps in Figs. 9–11 show that at a given time the polarity of the jerk amplitude varies across the globe thus we consider the trends in smaller regions of observatories where the same polarity signal would be expected. We focus on Europe and North America since these two regions provide the greatest coverage both in terms of numbers of observatories (29 and 27, respectively) and time spans of data.

We find that for both Europe and North America, in all three components, the jerk amplitude polarity can be seen to vary through time (Figs. 13(a–c) and 14(a–c)). In both regions, for all components these variations are zero mean to within a tolerance of ± 1 nT/yr² although distinct clustering of events in time and amplitude is stronger in Europe than in North America as the histograms in Fig. 7(a and c) show.

To assess the possible periodicity in jerk amplitudes we estimate the power spectra of the jerk amplitudes via the Lomb-Scargle method of least-squares spectral analysis (see Lomb, 1976; Scargle, 1982). It can be seen (Figs. 13(d–f) and 14(d–f)) that there are predominant peaks in the spectra, which synthetic testing indicates are not artefacts of the irregular time sampling of the jerk amplitudes. The statistical significance (α) of peaks in the spectra

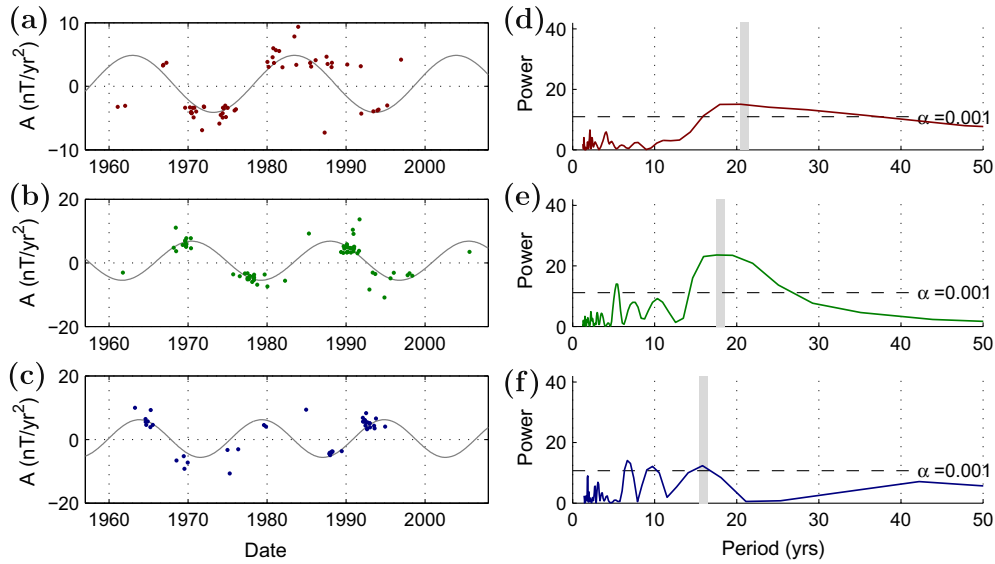


Fig. 13. Time series of jerk amplitudes for all European observatories (a–c) and corresponding power spectra calculated as Lomb-Scargle periodograms (d–f). Plot rows show X-, Y- and Z-components from top to bottom. Symbol α represents the statistical certainty level as a function of power with higher power more certain. Jerks were detected using the 10-yr window. The highlighted periods in (d–f) are plotted as least-square fit sinusoids over the data in (a–c).

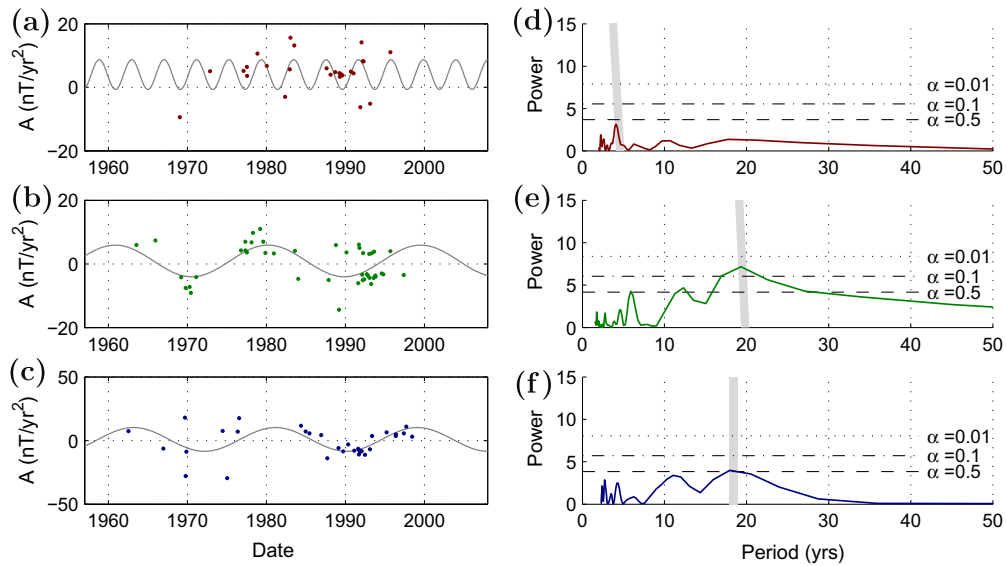


Fig. 14. As Fig. 13 but for all North American observatories.

is judged as a function of power derived from the exponential probability distribution of the spectrum, the number of frequencies tested and the oversampling factor (see Press et al., 2007). Thus higher power and lower values of α represent more certain results. Generally the spectra for Europe were found to hold more significant peaks than those for North America. It is possible that the length of the identification window used to calculate the linear regression creates artifacts in the periodicity of the identified jerk events. While no spectral peaks appear at aliased window periods, only signals which appear consistently in results from the 5-, 10-, 15- and 20-yr windows are considered robust observations.

European observatories were found to show significant, consistent signals for all detection window lengths at periods of ~ 18 – 20 yrs in the Y-component. Significant signals for three of the four window lengths were seen at ~ 17 – 20 yrs in the X-component, ~ 7 – 8 yrs in the Y-component, and ~ 7 yrs and ~ 15 – 16 yrs in the Z-component. North American observatories were not found to show

consistent signals at all detection window lengths but moderately significant signals were seen for three of four window lengths at ~ 11 – 12 yrs and ~ 19 – 21 yrs in the Y-component and ~ 18 – 22 yrs in the Z-component. The greater uncertainty of results for North America may be attributed to the greater spatial extent of the observatories (and thus greater variation of signal) compared to the dense network in Europe.

With the limited data available it is hard to be conclusive as to the presence of periodic signals worldwide. However, the premise is an interesting one, perhaps complementary to the ~ 6 -yr magnetic and LOD signals (or higher harmonics of) reported by Gillet et al. (2010), Silva et al. (2012) and Abarco del Rio et al. (2000). Periodicity in the polarity of jerk amplitudes implies that the observed step changes in the SA associated with jerks regularly oscillate between a similar maximum and minimum magnitude. This suggests that the source mechanism for the jerk signal is periodic and shows a relatively consistent magnitude effect in the observed

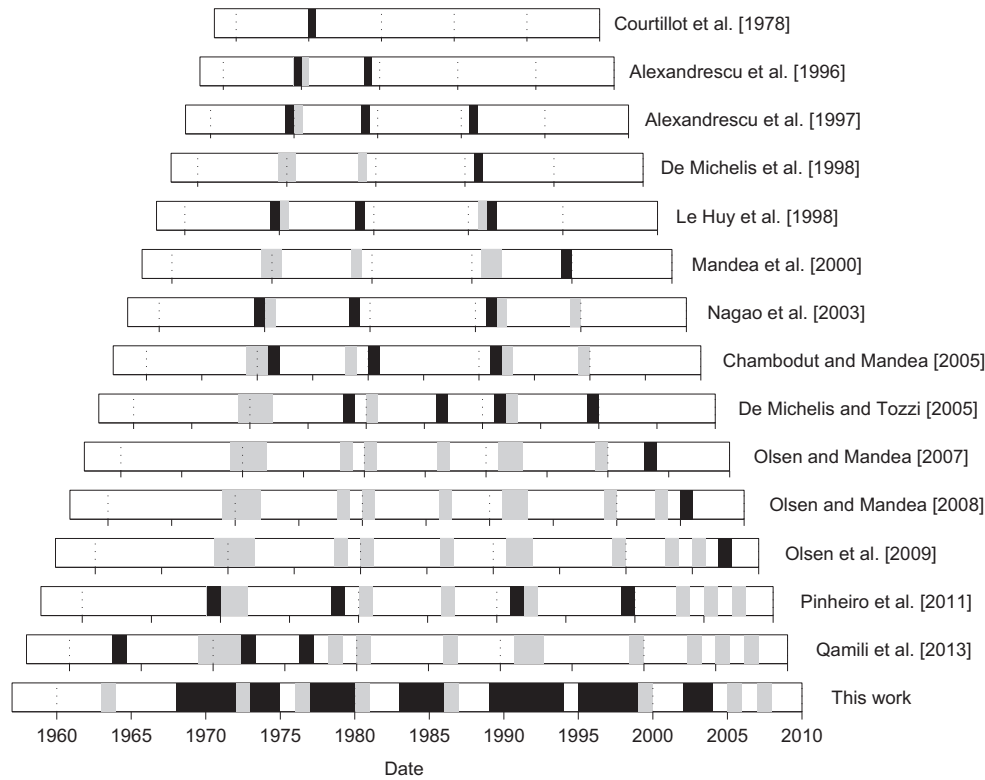


Fig. 15. Summary of identified jerks in selected publications. Black boxes represent jerks discussed in each particular publication, grey boxes show an amalgamation of the events from all works prior to a given publication. For the results of this work, the black boxes represent relative peaks in numbers of global jerk identifications while for all previous studies the boxes indicate the quoted mean year of identified jerks.

magnetic field in a given region. It has yet to be determined if the disparities in the periodicity observed between European and North American observatories persist to the core mantle boundary as a feature of the source mechanism or are an effect resulting from interaction with a conducting mantle (e.g. Pinheiro and Jackson, 2008).

5. Conclusions

The jerk identification method developed here proves to be a useful tool in the assessment of geomagnetic jerks in observatory data. Applying our specified detection criteria, requiring minimal *a priori* information, leads to the robust identification of all events which exhibit the characteristic form of a jerk in the SV. The technique also allows the variation of the selection criteria to assess the effects of the scale and definition of a jerk that is imposed. Using monthly mean data and removing external field signals produces increased time resolution and reduced uncertainty estimates on jerk occurrence times and amplitudes compared to the results of Pinheiro et al. (2011). Combined with relative probabilities for each event identified, the method provides a means to temper the certainty of each observation to assess how well our observations are constrained by the data.

The results presented here suggest that the established global and local jerk times reported in previous studies do not fully characterise the observations as a whole but rather describe select portions of a much larger data set. It should be noted that observatory data provide a very sparse data set for even the best observed events and that this should be taken into consideration when assessing the potential occurrence of global events. Nevertheless our observations suggest that between the epochs of 1957 and 2008 there are periods when jerks occur more frequently in partic-

ular regions of the world (Fig. 15). These can be summarised as 1968–71, 1973–74, 1977–79, 1983–85, 1989–93, 1995–98 and 2002–03 with the suggestion of further poorly sampled events in the early 1960s and late 2000s. It should be noted that none of these events were detected at more than 30% of observatories in a given year. These peaks in jerk occurrences do not appear to manifest as consistent forms in the distribution of amplitudes and are seen to occur in various combinations of components. Jerks are not seen to occur simultaneously across all regions of the globe and the bias of the data set to the Northern Hemisphere, particularly Europe, is evident in the composition of global jerk occurrences. Neither do jerks show a consistent relationship in patterns of occurrence between regions, which suggests that the relationship between so called jerk delay times and properties such as mantle electrical conductivity do not follow a simple or constant rule if at all. Better understanding of the cause of jerks may be needed to explain the variations in occurrence times observed.

Our results suggest that previously reported observations of jerks are largely consistent with our findings but restricted to those events of greatest magnitude and isolation in time. We show that event occurrences are frequent and occurrence patterns vary but that there are times when many events are seen in several components across large portions of the Earth's surface. The jerks detected around 1968–1971 stand out as being of significantly greater magnitude and the most isolated in time making their identification more robust and consistent. The general trend of increased numbers of identified jerks towards the end of the 20th century and start of the 21st century makes defining individual events more complicated as the distinction between 'early' and 'late' events blurs considerably. Again, analysis of the resulting magnetic field without comprehension of the source mechanism can only lead so far.

Our analyses of the spatial distributions of jerk amplitudes fit well with the observations of previous studies (e.g. Le Huy et al., 1998; De Michelis et al., 2000; Pinheiro et al., 2011) and suggest that our observations of less commonly reported events may help to expand the catalogue of features which must be explained by works addressing core dynamics.

To this end we present our final result, the possibility of periodicity in jerk amplitudes. The periodicities in time and magnitude of jerks observed in Europe and North America suggest potential links to other observed periods in the magnetic field, length-of-day and potential generation mechanisms (Gillet et al., 2010; Silva et al., 2012). Observing the jerk amplitude polarity and magnitude through time also provides a means of defining peaks in jerk occurrences and separating events which appear to overlap in time. The presence of several signals with varying periods in each component suggests that the source mechanism is far from simple. Additionally, there may be superposition of many signals and potentially interaction with mantle electrical conductivity variations to create the complicated spatial and temporal observations.

Acknowledgements

The results presented here rely on data collected at magnetic observatories. We thank the national institutes that support them, INTERMAGNET for promoting high standards of magnetic observatory practice (<http://www.intermagnet.org>) and the WDC for Geomagnetism at BGS, Edinburgh. We would like to thank Richard Holme whose review helped to improve the manuscript and Ingo Wardinski for valuable comments during the development of this work. This study was funded by NERC grants NE/I012052/1 and NE/G014043/1.

Appendix A. Supplementary data

Supplementary data associated with this article can be found, in the online version, at <http://dx.doi.org/10.1016/j.pepi.2013.06.001>.

References

- Abarco del Rio, R., Gambis, D., Salstein, D.A., 2000. Interannual signals in length of day and atmospheric angular momentum. *Ann. Geophys.* 18 (3), 347–364.
- Alexandrescu, M., Courtillot, V., Le Mouél, J.-L., 1997. High-resolution secular variation of the geomagnetic field in western Europe over the last 4 centuries: comparison and integration of historical data from Paris and London. *J. Geophys. Res.* 102 (B9), 20245–20258.
- Alexandrescu, M., Gibert, D., Hulot, G., Le Mouél, J.-L., Saracco, G., 1995. Detection of geomagnetic jerks using wavelet analysis. *J. Geophys. Res.* 100 (B7), 12557–12572.
- Alexandrescu, M., Gibert, D., Hulot, G., Le Mouél, J.-L., Saracco, G., 1996. Worldwide wavelet analysis of geomagnetic jerks. *J. Geophys. Res.* 101 (B10), 21975–21994.
- Allredge, L., 1984. A discussion of impulses and jerks in the geomagnetic-field. *J. Geophys. Res.* 89 (NB6), 4403–4412.
- Bloxham, J., Zatman, S., Dumberry, M., 2002. The origin of geomagnetic jerks. *Nature* 420 (6911), 65–68.
- Chambodut, A., Manda, M., 2005. Evidence for geomagnetic jerks in comprehensive models. *Earth Planets Space* 57 (2), 139–149.
- Chulliat, A., Telali, K., 2007. World monthly means database project. *Publ. Inst. Geophys. Pol. Acad. Sci. C-99* (398). Available at: <<http://www.bcmt.fr/wmmd.html>>..
- Chulliat, A., Thébaud, E., Hulot, G., 2010. Core field acceleration pulse as a common cause of the 2003 and 2007 geomagnetic jerks. *Geophys. Res. Lett.* 37.
- Courtillot, V., Ducruix, J., Le Mouél, J.-L., 1978. Sur une accélération récente de la variation séculaire du champ magnétique terrestre. *C. R. Acad. Sci. D* 287, 1095–1098.
- Daglis, I.A., Thorne, R.M., Baumjohann, W., Orsini, S., 1999. The terrestrial ring current: origin, formation, and decay. *Rev. Geophys.* 34 (7), 407–438.
- De Michelis, P., Cafarella, L., Meloni, A., 1998. Worldwide character of the 1991 geomagnetic jerk. *Geophys. Res. Lett.* 25 (3), 377–380.
- De Michelis, P., Cafarella, L., Meloni, A., 2000. A global analysis of the 1991 geomagnetic jerk. *Geophys. J. Int.* 143 (3), 545–556.
- De Michelis, P., Tozzi, R., 2005. A Local Intermittency Measure (LIM) approach to the detection of geomagnetic jerks. *Earth Planet. Sci. Lett.* 235 (1–2), 261–272.
- Gibert, D., Le Mouél, J.-L., 2008. Inversion of polar motion data: Chandler wobble, phase jumps, and geomagnetic jerks. *J. Geophys. Res.* 113 (B10).
- Gillet, N., Jault, D., Canet, E., Fournier, A., 2010. Fast torsional waves and strong magnetic field within the Earth's core. *Nature* 465, 74–77.
- Gubbins, D., Tomlinson, L., 1986. Secular variation from monthly means from Apia and Amberley magnetic observatories. *Geophys. J. Int.* 86 (2), 603–615.
- Holme, R., de Viron, O., 2005. Geomagnetic jerks and a high-resolution length-of-day profile for core studies. *Geophys. J. Int.* 160 (2), 435–439.
- Korte, M., Manda, M., Matzka, J., 2009. A historical declination curve for Munich from different data sources. *Phys. Earth Planet. Inter.* 177 (3–4), 161–172.
- Le Huy, M., Alexandrescu, M., Hulot, G., Le Mouél, J.-L., 1998. On the characteristics of successive geomagnetic jerks. *Earth Planets Space* 50 (9), 723–732.
- Le Mouél, J.-L., Ducruix, J., Duyen, C., 1982. The worldwide character of the 1969–1970 impulse of the secular acceleration rate. *Phys. Earth Planet. Inter.* 28 (4), 337–350.
- Lomb, N.R., 1976. Least-squares frequency analysis of unequally spaced data. *Astrophys. Space Sci.* 39 (2), 447–462.
- Malin, S.R.C., Hodder, B.M., 1982. Was the 1970 geomagnetic jerk of internal or external origin? *Nature* 296 (5859), 726–728.
- Malin, S.R.C., Hodder, B.M., 1982. Was the 1970 geomagnetic jerk of internal or external origin? *Geophys. J. Int.* 69 (1), 289.
- Manda, M., Bellanger, E., Le Mouél, J.-L., 2000. A geomagnetic jerk for the end of the 20th century? *Earth Planet. Sci. Lett.* 183 (3–4), 369–373.
- Manda, M., Holme, R., Pais, A., Pinheiro, K., Jackson, A., Verbanac, G., 2010. Geomagnetic jerks: rapid core field variations and core dynamics. *Space Sci. Rev.* 155 (1–4), 147–175.
- Mayaud, P.N., 1980. Derivation, Meaning, and Use of Geomagnetic Indices. No. 22 in *Geophysical Monograph*. American Geophysical Union, Washington, DC.
- Nagao, H., Iyemori, T., Higuchi, T., Araki, T., 2003. Lower mantle conductivity anomalies estimated from geomagnetic jerks. *J. Geophys. Res.* 108 (B5).
- Olsen, N., Manda, M., 2007. Investigation of a secular variation impulse using satellite data: the 2003 geomagnetic jerk. *Earth Planet. Sci. Lett.* 255 (1–2), 94–105.
- Olsen, N., Manda, M., 2008. Rapidly changing flows in the Earth's core. *Nat. Geosci.* 1 (6), 390–394.
- Olsen, N., Manda, M., Sabaka, T.J., Tffner-Clausen, L., 2009. CHAOS-2-a geomagnetic field model derived from one decade of continuous satellite data. *Geophys. J. Int.* 179 (3), 1477–1487.
- Pinheiro, K., Jackson, A., 2008. Can a 1-D mantle electrical conductivity model generate magnetic jerk differential time delays? *Geophys. J. Int.* 173 (3), 781–792.
- Pinheiro, K.J., Jackson, A., Finlay, C.C., 2011. Measurements and uncertainties of the occurrence time of the 1969, 1978, 1991, and 1999 geomagnetic jerks. *Geochim. Geophys. Geosyst.* 12.
- Press, W.H., Teukolsky, S.A., Vetterling, W.T., Flannery, B.P., 2007. *Numerical Recipes: The Art of Scientific Computing*, third ed. Cambridge University Press, pp. 685–692 (Chapter 13.8).
- Qamili, E., De Santis, A., Isac, A., Manda, M., Duka, B., Simonyan, A., 2013. Geomagnetic jerks as chaotic fluctuations of the Earth's magnetic field. *Geochim. Geophys. Geosyst.* 14 (4), 839–850.
- Sabaka, T., Olsen, N., Purucker, M., 2004. Extending comprehensive models of the Earth's magnetic field with Orsted and CHAMP data. *Geophys. J. Int.* 159 (2), 521–547.
- Scargle, J.D., 1982. Studies in astronomical time series analysis II. Statistical aspects of spectral analysis of unevenly sampled data. *Astrophys. J.* 263, 835–853.
- Silva, L., Hulot, G., 2012. Investigating the 2003 geomagnetic jerk by simultaneous inversion of the secular variation and acceleration for both the core flow and its acceleration. *Phys. Earth Planet. Inter.* 198, 28–50.
- Silva, L., Jackson, L., Mound, J., 2012. Assessing the importance and expression of the 6-year geomagnetic oscillation. *J. Geophys. Res.* 117 (B10101).
- Stewart, D., Whaler, K., 1995. Optimal piecewise regression-analysis and its application to geomagnetic time-series. *Geophys. J. Int.* 121 (3), 710–724.
- Verbanac, G., Lühr, H., Rother, M., Korte, M., Manda, M., 2007. Contributions of the external field to the observatory annual means and a proposal for their corrections. *Earth Planets Space* 59 (4), 251–257.
- Wardinski, I., Holme, R., 2011. Signal from noise in geomagnetic field modelling: denoising data for secular variation studies. *Geophys. J. Int.* 185 (2), 653–662.
- Wardinski, I., Lesur, V., 2012. An extended version of the C3FM geomagnetic field model: application of a continuous frozen-flux constraint. *Geophys. J. Int.* 189 (3), 1409–1429.